The Screen representation of spin networks: 2D recurrence, eigenvalue equation for $6j$ symbols, geometric interpretation and Hamiltonian dynamics.

Roger W. Anderson[1], Vincenzo Aquilanti[2,3], Ana Carla P. Bitencourt[4], Dimitri Marinelli[5,6], and Mirco Ragni[4]

[1] Department of Chemistry, University of California, Santa Cruz, CA 95064, U.S.A.
anderso@ucsc.edu
[2] Dipartimento di Chimica, Università di Perugia, Italy
vincenzoaquilanti@yahoo.it
[3] Istituto Metodologie Inorganiche e Plasmi CNR, Roma, Italy
[4] Departamento de Física, Universidade Estadual de Feira de Santana, Brazil
[5] Dipartimento di Fisica, Università degli Studi di Pavia, Italy
[6] INFN, sezione di Pavia, 27100 Pavia, Italy

Abstract. This paper treats $6j$ symbols or their orthonormal forms as a function of two variables spanning a square manifold which we call the "screen". We show that this approach gives important and interesting insight. This two dimensional perspective provides the most natural extension to exhibit the role of these discrete functions as matrix elements that appear at the very foundation of the modern theory of classical discrete orthogonal polynomials. Here we present 2D and 1D recursion relations that are useful for the direct computation of the orthonormal $6j$, which we name U. We present a convention for the order of the arguments of the $6j$ that is based on their classical and Regge symmetries, and a detailed investigation of new geometrical aspects of the $6j$ symbols. Specifically we compare the geometric recursion analysis of Schulten and Gordon with the methods of this paper. The 1D recursion relation, written as a matrix diagonalization problem, permits an interpretation as a discrete Shrödinger-like equations and an asymptotic analysis illustrates semiclassical and classical limits in terms of Hamiltonian evolution.

1 Introduction

Continuing and extending previous work [1,2,3,4] on $6j$ symbols, (or on the equivalent Racah coefficients), of current use in quantum mechanics and recently also of interest as the elementary building blocks of spin networks [5,6,7], in this paper we *(i)* - adopt a representation (the "screen") accounting for exchange and Regge symmetries; *(ii)* - introduce a recurrence relationship in two variables, allowing not only a computational algorithm for the generation of the $6j$ symbols to be plotted on the screen, but also representing a partial difference equation

allowing us to interpret the dynamics of the two dimensional system. *(iii)* - introduce a recurrence relationship as an equation in one variable, extending the known ones which are also computationally interesting; *(iv)* - give a formulation of the difference equation as a matrix diagonalization problem, allowing its interpretation as a discrete Schrödinger equation; *(v)* - discuss geometrical and dynamical aspects from an asymptotic analysis. We do not provide here detailed proofs of these results, but give sufficient hints for the reader to work out the derivations. For some of the topics we refer to a recent problem recently tackled [8]; numerical and geometrical illustrations are presented on a companion paper [9]. A concluding section introduces aspects of relevance for the general spin networks by sketching some features of the $9j$ symbols.

2 The screen: Classical and Regge symmetries, Canonical Form

The Wigner $6j$ symbols $\left\{ \begin{matrix} j_1 & j_2 & j_{12} \\ j_3 & j & j_{23} \end{matrix} \right\}$ are defined as a matrix element beetween alternative angular momentum coupling schemes [10] by the relation

$$\langle j_1 j_2 \left(j_{12} \right) j_3 j m \mid j_1 j_2 j_3 \left(j_{23} \right) j' m' \rangle = (-1)^{j_1 + j_2 + j_3 + j} \, \delta_{jj'} \delta_{mm'} U \left(j_1 j_2 j j_3 ; j_{12} j_{23} \right),$$

where the orthonormal transformation U is

$$U \left(j_1 j_2 j j_3 ; j_{12} j_{23} \right) = \sqrt{(2 j_{12} + 1)(2 j_{23} + 1)} \left\{ \begin{matrix} j_1 & j_2 & j_{12} \\ j_3 & j & j_{23} \end{matrix} \right\} \tag{1}$$

For given values of j_1, j_2, j_3, and j the U will be defined over a range for both j_{12} and j_{23}. These ranges are given by

$$
\begin{aligned}
j_{12 \; min} &= \max \left(\mid j_1 - j_2 \mid, \mid j - j_3 \mid \right), & j_{12 \; max} &= \min \left(j_1 + j_2, j + j_3 \right), \\
j_{23 \; min} &= \max \left(\mid j_1 - j \mid, \mid j_2 - j_3 \mid \right), & j_{23 \; max} &= \min \left(j_1 + j, j_2 + j_3 \right), \\
\text{and} \quad & j_{12 \; min} \le j_{12} \le j_{12 \; max}, & j_{23 \; min} &\le j_{23} \le j_{23 \; max}.
\end{aligned}
\tag{2}
$$

The screen corresponds to the $6j$ or, as we specify below, the U values for all possible values of j_{12} and j_{23} .

The range for j_{12} and j_{23} is determined by the values of the independent variables: j_1, j_2, j_3, and j. In the remainder of this paper we make this clear by introducing new variables a, b, c, d, x and y to replace the j values. We specify the new variables by establishing a correspondence:

$$\left\{ \begin{matrix} a & b & x \\ c & d & y \end{matrix} \right\} \Leftrightarrow \left\{ \begin{matrix} j_1 & j_2 & j_{12} \\ j_3 & j & j_{23} \end{matrix} \right\} \tag{3}$$

Assuming that x and y remain respectively in the upper and lower right side of the $6j$ symbols, there are four classical and one Regge relevant symmetries:

$$\left\{ \begin{matrix} a & b & x \\ c & d & y \end{matrix} \right\} = \left\{ \begin{matrix} b & a & x \\ d & c & y \end{matrix} \right\} = \left\{ \begin{matrix} d & c & x \\ b & a & y \end{matrix} \right\} = \left\{ \begin{matrix} c & d & x \\ a & b & y \end{matrix} \right\} = \left\{ \begin{matrix} s-a & s-b & x \\ s-c & s-d & y \end{matrix} \right\}, \tag{4}$$

where $s = (a + b + c + d)/2$. It can be shown [2,1] that $x_{max} - x_{min} = y_{max} - y_{min} = 2\min(a, b, c, d, s - d, s - c, s - b, s - a) = 2\kappa$. The square screen will contain $(2\kappa + 1)^2$ values. The canonical ordering for $6j$ screens can now be specified by considering the two sets of values: a, b, c, d and its Regge transform $a' = s - a$, $b' = s - b$, $c' = s - c$, and $d' = s - d$. Take the set with the smallest entry and use the classical $6j$ symmetries to place this smallest value in the upper left corner of the $6j$ symbol. The placement of the other $6j$ arguments are determined by the symmetry relations. The resulting symbol has the property that $x_{\min} = b - a \leq x \leq b + a = x_{\max}$ and $y_{\min} = d - a \leq y \leq d + a = y_{\max}$. Furthermore we require that $a \leq b \leq d$ for the Canonical form. This may require using Eq. 5 to "orient" the screen in this way.

$$\begin{Bmatrix} a\ b\ x \\ c\ d\ y \end{Bmatrix} = \begin{Bmatrix} a\ d\ y \\ c\ b\ x \end{Bmatrix} \tag{5}$$

It can be shown that any symbol to be studied as a function of two entries can be reduced to the canonical form of Eq. 5 where $a \leq b \leq d \leq b + c - a$ and $c_{\min} = d - a + b \leq c \leq d + a - b = c_{\max}$.

Regge transformation for the parameters of the screen is a linear $O(4)$ transformation:

$$\frac{1}{2} \begin{pmatrix} -1 & 1 & 1 & 1 \\ 1 & -1 & 1 & 1 \\ 1 & 1 & -1 & 1 \\ 1 & 1 & 1 & -1 \end{pmatrix} \begin{pmatrix} a \\ b \\ c \\ d \end{pmatrix} = \begin{pmatrix} s - a \\ s - b \\ s - c \\ s - d \end{pmatrix}. \tag{6}$$

It can be checked that several functions appearing below (caustics, ridges, etc.) are invariant under such symmetry and also when represented on the screen (See [9]).

3 Tetrahedra and $6j$ symbols

In the following when we consider $6j$ properties as correlated to those of the tetrahedron of Figure 1a [3], we use the substitutions $A = a + 1/2$, $B = b + 1/2$, $C = c + 1/2$, $D = d + 1/2$, $X = x + 1/2$, $Y = y + 1/2$ which greatly improves all asymptotic formulas down to surprisingly low values of the entries. We show the argument ranges where the correspondence with the tetrahedron breaks down in section 5.2.

The area of each triangular face is given by the Heron formula:

$$F(A, B, C) = \frac{1}{4}\sqrt{(A + B + C)(-A + B + C)(A - B + C)(A + B - C)} \tag{7}$$

where A, B, C are the sides of the face. Upper case letters are used here to stress that geometric lengths are used in the equation. The square of the area can be also expressed as a Cayley-Menger determinant. Similarly, the square of the volume of an irregular tetrahedron, can also be written as a Cayley-Menger

determinant (Eq. 8 or as a Gramian determinant [11]. The latter determinant embodies a clearer relationship with a vectorial picture but with partial spoiling of the symmetry.

$$V^2 = \frac{1}{288} \begin{vmatrix} 0 & C^2 & D^2 & Y^2 & 1 \\ C^2 & 0 & X^2 & B^2 & 1 \\ D^2 & X^2 & 0 & A^2 & 1 \\ Y^2 & B^2 & A^2 & 0 & 1 \\ 1 & 1 & 1 & 1 & 0 \end{vmatrix}. \tag{8}$$

An explicit formula, due to Piero della Francesca, will be used in the companion paper [9]. Additionally mirror symmetry [1], can be used to extend screens to cover a larger range of arguments. The appearance of squares of tetrahedron edges entails that the invariance with respect to the exchange $X \leftrightarrow -X$ implies formally $x \leftrightarrow -x - 1$ with respect to entries in the $6j$ symbol. Although this is physically irrelevant when the js are pseudo-vectors, such as physical spins or orbital angular momenta, it can be of interest for other (e.g. discrete algorithms) applications. Regarding the screen, it can be seen that actually by continuation of X and Y to negative values, one can have replicas that can be glued by cutting out regions shaded in Fig. in [12], allowing mapping onto the S^2 manifold.

Figure 1b illustrates V^2 for values of a, b, c, and d used later in this paper.
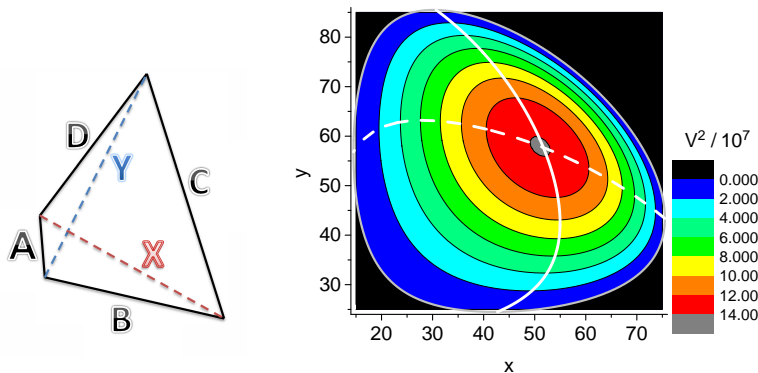
(a) Ponzano-Regge tetrahedron built with the six angular momenta in the $6j$ symbol.

(b) V^2 (contours for Eq. 8), caustics Eq. 12 (gray boundary), ridges (solid white Eq. 9, dashed Eq. 13) for $a = 30$, $b = 45$, $c = 60$, and $d = 55$.

Fig. 1

The following equations were first introduced in Refs. [1] and [3], but they are rewritten here with changed notation. When the values of A, B, C, D and

X are fixed, the maximum value for the volume as a function of Y is given by the "ridge" curve

$$Y^{Vmax} = \left(\frac{(A^2 - B^2)(C^2 - D^2) + (A^2 + B^2 + C^2 + D^2)X^2 - X^4}{2X^2} \right)^{1/2} \quad , \quad (9)$$

the corresponding volume is

$$V^{max}(A, B, C, D, X) = \frac{\sqrt{\Lambda_{A,B,X} \Lambda_{C,D,X}}}{24X} \quad , \quad (10)$$

where

$$\Lambda_{\alpha,\beta,\gamma} = \left(\alpha^2 - \beta^2\right)^2 - 2\gamma^2 \left(\alpha^2 + \beta^2\right) + \gamma^4. \quad (11)$$

Therefore the two values of Y for which the volume is zero are:

$$Y^z = \left(\left(Y^{Vmax}\right)^2 \pm \frac{\sqrt{\Lambda_{A,B,X} \Lambda_{C,D,X}}}{2X^2} \right)^{1/2}. \quad (12)$$

The values for Y^z mark the boundaries between classical and nonclassical regions, and therefore called "caustics".

Also when the values of A, B, C, D and Y are fixed, the maximum value for the volume as a function of X is given by the other "ridge" curve:

$$X^{Vmax} = \left(\frac{(A^2 - D^2)(C^2 - B^2) + (A^2 + B^2 + C^2 + D^2)Y^2 - Y^4}{2Y^2} \right)^{1/2} \quad . \quad (13)$$

4   Recursion formulas and exact calculations

The U values that are represented on the screen must be calculated by efficient and accurate algorithms, and we employed several methods that we have previously discussed and tested. Explicit formulas are available either as sums over a single variable and series, and we have used such calculations with multiple precision arithmetic in previous work [13],[3], [14], [15] . These high accuracy calculations are entirely reliable for all U that we have considered in the past, and the results provide a stringent test for other methods. However recourse to recursion formulas appears most convenient for fast accurate calculations and -as we will emphasize- also for semiclassical analysis, in order to understand high j limit and in reverse to interpret them as discrete wavefunctions obeying Schrödinger type of difference (rather than differential) equations.

The goal is to determine the elements of the ortho-normal transformation matrix:

$$U(x, y) = \sqrt{(2x + 1)(2y + 1)} \begin{Bmatrix} a & b & x \\ c & d & y \end{Bmatrix}. \quad (14)$$

Two approaches can be used to evaluate $U(x, y)$: evaluate the $6j$ from recursion formulas and then apply the normalization or to use direct calculation from explicit formulas.

4.1   2D (x,y) recursion for U

In this work, we first derive and computationally implement a two variable recurrence that permits construction of the whole orthonormal matrix The derivation follows our paper in [14] and is also of interest for other $3nj$ symbols.

By setting $h = 0$ in the formula 43 in section 6 , we obtain a five term recurrence relation for $U(x, y)$:

$$
\begin{aligned}
(-1)^{2x} &\sqrt{\frac{2x-1}{2y+1}} \begin{Bmatrix} b & x-1 & a \\ 1 & a & x \end{Bmatrix} \begin{Bmatrix} d & x-1 & c \\ 1 & c & x \end{Bmatrix} U(x-1, y) \\
&+(-1)^{2x} \sqrt{\frac{2x+1}{2y+1}} \begin{Bmatrix} b & x & a \\ 1 & a & x \end{Bmatrix} \begin{Bmatrix} d & x & c \\ 1 & c & x \end{Bmatrix} U(x, y) \\
+(-1)^{2x} &\sqrt{\frac{2x+3}{2y+1}} \begin{Bmatrix} b & x+1 & a \\ 1 & a & x \end{Bmatrix} \begin{Bmatrix} d & x+1 & c \\ 1 & c & x \end{Bmatrix} U(x+1, y) \\
=(-1)^{2y} &\sqrt{\frac{2y-1}{2x+1}} \begin{Bmatrix} b & y-1 & c \\ 1 & c & y \end{Bmatrix} \begin{Bmatrix} d & y-1 & a \\ 1 & a & y \end{Bmatrix} U(x, y-1) \\
&+(-1)^{2y} \sqrt{\frac{2y+1}{2x+1}} \begin{Bmatrix} b & y & c \\ 1 & c & y \end{Bmatrix} \begin{Bmatrix} d & y & a \\ 1 & a & y \end{Bmatrix} U(x, y) \\
+(-1)^{2y} &\sqrt{\frac{2y+3}{2x+1}} \begin{Bmatrix} b & y+1 & c \\ 1 & c & y \end{Bmatrix} \begin{Bmatrix} d & y+1 & a \\ 1 & a & y \end{Bmatrix} U(x, y+1) \quad (15)
\end{aligned}
$$

This recurrence relation Eq. 15 will yield the entire set of $U(x, y)$ that constitute the screen. Replacing the $6j$ symbols of unit argument with the algebraic expressions in Varshalovich [10], we obtain an effective method to calculate the screen.

5   1D (x) symmetric recursion for U

Starting with the recurrence relation in Neville [16] and Schulten and Gordon [17] for the $6j$ and carefully converting it into a recurrence relation for U, we can write a three term symmetric recursion relationship, which is here conveniently represented as an eigenvalue equation:

$$
p_+ (x) U (x+1, y) + w(x) U (x, y) + p_- (x) U (x-1, y) = \lambda (y) U (x, y) , \quad (16)
$$

where

$$
\begin{aligned}
p_+ (x) = &\{(a+b+x+2)(a+b-x)(a-b+x+1)(-a+b+x+1)\}^{\frac{1}{2}} \\
&\times \{(d+c+x+2)(d+c-x)(d-c+x+1)(-d+c+x+1)\}^{\frac{1}{2}} \quad (17) \\
&\times (x+1)^{-1} [(2x+1)(2x+3)]^{-\frac{1}{2}}
\end{aligned}
$$

$$p_-(x) = p_+(x-1) \tag{18}$$

$$w(x) = [b(b+1) - a(a+1) + x(x+1)]$$
$$\times [d(d+1) - c(c+1) - x(x+1)] / [x(x+1)] \tag{19}$$

$$\lambda(y) = 2[y(y+1) - b(b+1) - c(c+1)] . \tag{20}$$

For convenience we can also define:

$$w_\lambda = w(x) - \lambda(y) \tag{21}$$

A row of the screen may be efficiently and accurately calculated from these equations. Diagonalization of the symmetric tridiagonal matrix given by the $p_+(x)$, $w(x)$, $p_-(x)$ provides an accurate check: the eigenvalues of the tridiagonal matrix precisely match those expected from Eq. 20 and eigenvectors generate $U(x,y)$. Stable results are obtained with double precision arithmetic.

5.1 Potential functions and Hamiltonian dynamics

For the eigenvalue equation (Eq. 16), interpreted as discrete Schrödinger-like equation, two potentials $\mathbf{W}^+(x)$ and $\mathbf{W}^-(x)$ can be defined:

$$\mathbf{W}^\pm(x) = w(x) \pm 2 \mid p(x) \mid, \tag{22}$$

where [18]

$$p(x) = \frac{1}{2}(p_+(x) + p_-(x)) \tag{23}$$

or [19]

$$p(x) = \sqrt{(p_+(x) \, p_-(x))}. \tag{24}$$

The two definitions agree well except for x near the limits x_{min} or x_{max}. With the second choice for $\bar{p}(x)$ the values for $\mathbf{W}^\pm$ are the same at the limits, but there are differences with the first choice. See the figures 2a and 2b. Compare with Ref. [8] where Hamiltonian dynamics is developed for a similar system. Braun's potential functions are closely related to the caustics illustrated in [1] and [9].

5.2 Geometric interpretation

The geometrical interpretations of the $6j$ symbols provide fundamental understanding and important semiclassical limits. This approach originates from Ponzano and Regge [20] and elaborated by others, notably Schulten and Gordon [17].

The three-term recursion relationship (Eq. 16), for U admits an illustration in terms of a geometric interpretation: with some approximations to be detailed below one has finite difference equations (see Ref.[16], Eq.(67) for relationships
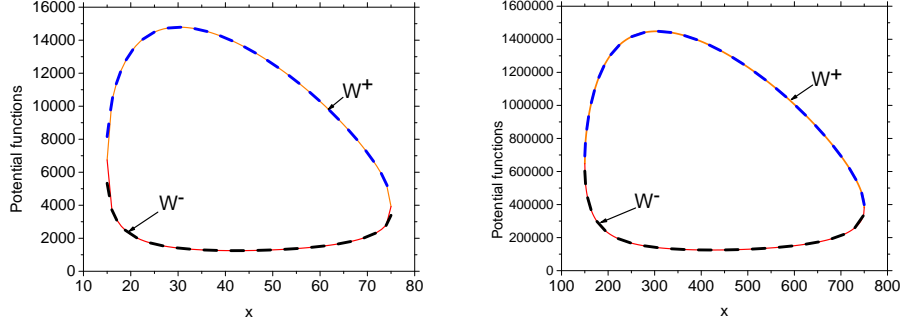
(a) Angular momenta corresponding to Figure 1b

(b) Angular momenta: $a = 300$, $b = 450$, $c = 600$, and $d = 550$.

Fig. 2: Potential functions corresponding to Eq. 23 (dashed blue and black lines) and Eq.24 (thin solid orange and red lines)

between recursions and finite difference), Consider the Schulten-Gordon relationships Eq.(66) and Eq.(67)(Ref. [17]). Here we show new geometric representations of the recursion relationships.

By setting $a = A - \frac{1}{2}$, $b = B - \frac{1}{2}$, $c = C - \frac{1}{2}$, $d = D - \frac{1}{2}$, $x = X - \frac{1}{2}$, and $y = Y - \frac{1}{2}$ one can write Eq. 16 in terms of triangle areas, a length X', and the cosine of a dihedral angle θ_3. The accuracy of this approximation is excellent, and depends slightly on the choice for X'.

$$
\frac{F(X - \frac{1}{2}, A, B)F(X - \frac{1}{2}, C, D)}{\left(X - \frac{1}{2}\right)^2} U\left(x - 1, y\right)
$$

$$
+\frac{F(X + \frac{1}{2}, A, B)F(X + \frac{1}{2}, C, D)}{\left(X + \frac{1}{2}\right)^2} U\left(x + 1, y\right)
$$

$$
-2\cos\theta_3 \frac{F(X', A, B)F(X', C, D)}{X'^2} U\left(x, y\right) \approx 0 \tag{25}
$$

and Eq.(69)[17]

$$
\cos\theta_3 = \frac{2X'^2 Y^2 - X'^2\left(-X'^2 + D^2 + C^2\right) - B^2\left(X'^2 + D^2 - C^2\right) - A^2\left(X'^2 - D^2 + C^2\right)}{16F\left(X', B, A\right)F\left(X', D, C\right)}, \tag{26}
$$

where $F(a, b, c)$ is "area" of abc triangle (Eq. 7). (This recursion relation Eq. 25 must be multiplied through by 8 to compare precisely with Eq. 16.

Here we consider two choices for X' in Eq. 19:

$$
X'^2 = \left(X - \frac{1}{2}\right)\left(X + \frac{1}{2}\right) = X^2 - \frac{1}{4}, \tag{27}
$$

$$
X' = X \tag{28}
$$

The first choice (Eq. 27) provides an almost exact approximation to Eqns. 17, 18,19, and 20 Coefficients in Eq. 16. The second Eq. 28 uses only integer or half integer arguments, and for most X works as well as the first. The figures 3a and 3b show the errors and their significance. In these figures $w_\lambda\,(approx)$ is specified as:

$$w_\lambda\,(approx) = -2\cos\theta_3 \frac{F(X',A,B)F(X',C,D)}{X'^2} \tag{29}$$

For either choice of X', the recursion coefficients are connected to the geometry of tetrahedra [20]:

$$\frac{3}{2}VX' = F(X',A,B)F(X',C,D)\sin\theta_3 \ , \tag{30}$$

where V is the tetrahedral volume.

Equations 25 can be recast by the geometric mean approximation:

$$\frac{F(X\pm\frac{1}{2},A,B)}{\left(X\pm\frac{1}{2}\right)} \simeq \frac{\sqrt{F(X\pm 1,A,B)F(X,A,B)}}{\sqrt{X\,(X\pm 1)}}, \tag{31}$$

where A and B can be also replaced by C and D.

With Eq. 31 Eq. 25 becomes:

$$\frac{\sqrt{F(X-1,A,B)F(X,A,B)F(X-1,C,D)F(X,C,D)}}{X\,(X-1)}U\,(x-1,y)$$

$$+\frac{\sqrt{F(X+1,A,B)F(X,A,B)F(X+1,C,D)F(X,C,D)}}{X\,(X+1)}U\,(x+1,y)$$

$$-2\cos\theta_3\frac{F(X,A,B)F(X,C,D)}{X^2}U\,(x,y) \approx 0, \tag{32}$$

This equation is useful, but definitely less accurate than Eq. 25 (See Figures 4a and 4b).

With cancellation of terms in X, this Eq. 32 becomes:

$$\frac{\sqrt{F(X-1,A,B)F(X-1,C,D)}}{(X-1)}U\,(x-1,y)$$

$$+\frac{\sqrt{F(X+1,A,B)F(X+1,C,D)}}{(X+1)}U\,(x+1,y)$$

$$-2\cos\theta_3\frac{\sqrt{F(X,A,B)F(X,C,D)}}{X}U\,(x,y) \approx 0. \tag{33}$$

This is equivalent to the recursion relation of Schulten and Gordon [17], that they use to establish their semiclassical approximations for $6j$ symbols. Their equation is accurate enough for $x_{min} \ll x \ll x_{max}$, but not so accurate near the limits.

In terms of the finite difference operator, Eq. 32 becomes after using Eq. 30: $\Delta^2(x)f(x) = f(x+1) - 2f(x) + f(x-1)$:

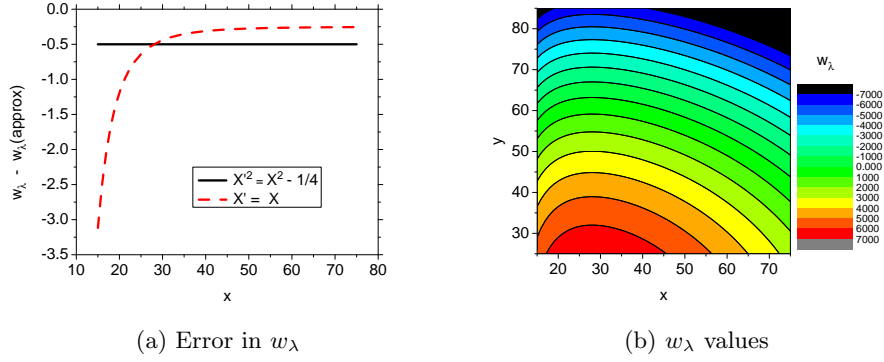$$[\Delta^2(X) + 2 - 2\cos\theta_3]f(X) \simeq 0 \ , \tag{34}$$

(a) Error in w_λ

(b) w_λ values

Fig. 3: Parameters a, b, c, d of Figure 1b

(a) Angular momenta of figure 1b
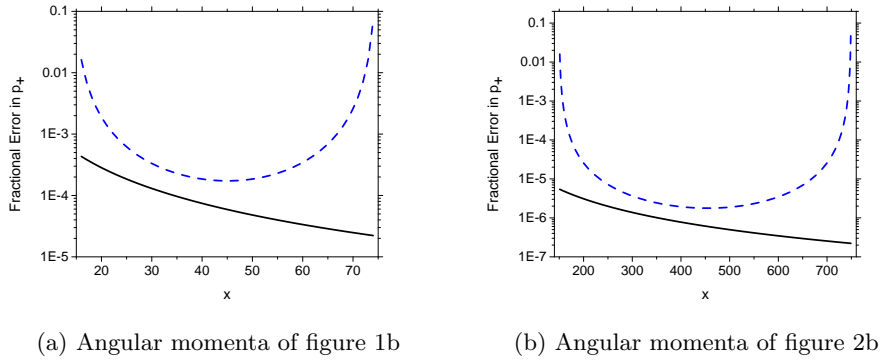
(b) Angular momenta of figure 2b

Fig. 4: Fractional errors in p_+ using Eq. 25, solid black line and Eq. 32, dashed blue line.

where

$$f(X) = \frac{\sqrt{F(X, A, B)F(X, C, D)}}{X} U(x, y) = \sqrt{\frac{V}{X \sin \theta_3}} U(x, y) \ . \tag{35}$$

We have, explicitly

$$\cos \theta_3 = \pm \sqrt{1 - \left(\frac{3VX}{2F(X, A, B)F(X, C, D)}\right)^2} \ . \tag{36}$$

Our Eq. 35 is only slightly different from that of Schulten and Gordon, because we have an extra X in the denominator of the definition of $f(X)$. This occurs because we use the recursion for U instead of that for $6j$.

5.3 Semiclassical approximation

The following developments parallel those in [3]. From the above formulas, and from that of the volume, we have that

- $V = 0$ implies $\cos \theta_3 = \pm 1$ and establishes the classical domain between X_{min} and X_{max}
- $F(X, A, B) = 0$ or $F(X, C, D) = 0$ establish the definition limits x_{min} and x_{max}.

For a Schrödinger type equation

$$\frac{d^2\psi}{dx^2} + p^2\psi = 0 \ , \qquad \hbar^2/2m = 1 \ , \tag{37}$$

its discrete analog in a grid having one as a step,

$$\psi_{n+1} + (p^2 - 2)\psi_n + \psi_{n-1} = 0, \tag{38}$$

and we then have after comparing Eq. 38 with Eq. 34

$$f(X + 1) - 2\cos \theta_3 f(X) + f(X - 1) = 0. \tag{39}$$

The identification

$$p = \pm(2 - 2\cos \theta_3)^{1/2} \tag{40}$$

is then evident. Here we present a x,y plot Fig. 5 of $1 - \cos \theta_3$ that clearly shows this definition of the classical region.

Evidentially, on the closed loop, we can enforce Bohr-Sommerfeld phase space quantization:

$$\oint p \, dx = (n + 1/2) \, \pi \ . \tag{41}$$

The eigenvalues n obtained in this way may be easily related to the allowed y. These formulas are illustrated in Fig. 6 and 7 of Ref [3].
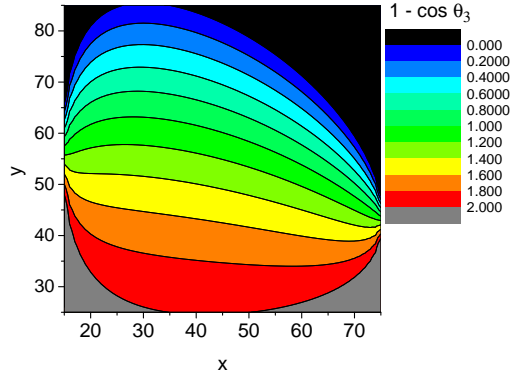
Fig. 5: x,y plot of $\cos\theta_3$ for angular momenta of Fig 1(b)

The Ponzano-Regge formula for the $6j$ in the classical region is

$$\begin{Bmatrix} a\ b\ x \\ c\ d\ y \end{Bmatrix} \approx \frac{1}{\sqrt{12\pi|V|}} \cos\left(\Phi\right),\tag{42}$$

where the Ponzano-Regge phase is: $\Phi = A\theta_1 + B\theta_2 + X\theta_3 + C\eta_1 + D\eta_2 + Y\eta_3 + \frac{\pi}{4}$. The angles are determined by rearranged equations: Eq. 30. The various dihedral angles are found from the equations in [20].

To the extent that the Ponzano-Regge approximation is valid we see that the $6j$ symbols have a magnitude envelop given by V and a phase that is a function of X and Y determined by Φ. Eq. 42 works quite well for X and Y well within the classical region. However its use near the caustics is limited because of two factors:

1. The approximate recursion relation given by Eq. 32 differs most from the exact recursion Eqs. 17,18,19,20 near the caustics.
2. The semiclassical approximation for the $6j$ also breaks down near the caustics.

For piece-wise extensions , see [20] and for uniformly valid formulas see [17].

6 $9j$ and higher spin networks

In this work, we first have derived and computationally implemented a two variable recurrence that permits construction of the whole orthonormal matrix The derivation follows our paper in [14] and is also of interest for other $3nj$ symbols.

We find in [14]; see also [10], the following 2D recurrence relationship for $9j$ symbols:

$$\frac{A_{c+1}(ab,fj)}{(c+1)(2c+1)} \begin{Bmatrix} a\ b\ c+1 \\ d\ e\ \ f \\ g\ h\ \ j \end{Bmatrix} + \frac{A_c(ab,fj)}{c(2c+1)} \begin{Bmatrix} a\ b\ c-1 \\ d\ e\ \ f \\ g\ h\ \ j \end{Bmatrix} - \frac{A_{d+1}(ef,ag)}{(d+1)(2d+1)} \begin{Bmatrix} a\ \ \ b\ c \\ d+1\ e\ f \\ g\ \ \ h\ j \end{Bmatrix}$$

$$-\frac{A_d(ef,ag)}{d(2d+1)} \begin{Bmatrix} a\ \ \ b\ c \\ d-1\ e\ f \\ g\ \ \ h\ j \end{Bmatrix} = \left[\frac{B_d(ag,fe)}{d(d+1)} - \frac{B_c(ab,jf)}{c(c+1)} \right] \begin{Bmatrix} a\ b\ c \\ d\ e\ f \\ g\ h\ j \end{Bmatrix}$$

$$A_q\left(pr,st\right) = \left[\left(-p+r+q\right)\left(p-r+q\right)\left(p+r-q+1\right)\left(p+r+q+1\right)\right]^{\frac{1}{2}}$$

$$\times\left[\left(-s+t+q\right)\left(s-t+q\right)\left(s+t-q+1\right)\left(s+t+q+1\right)\right]^{\frac{1}{2}}$$

$$B_q\left(pr,st\right) = \left[q\left(q+1\right)-p\left(p+1\right)+r\left(r+1\right)\right]\left[q\left(q+1\right)-s\left(s+1\right)+t\left(t+1\right)\right]$$

$$(43)$$

Geometrical interpretations of A's as proportional to products of areas of triangular faces and of B's as angular functions of associated structures, will serve for further work on the dynamical description of general spin networks. As noted in [14], Eq. 15 can be derived by setting $h = 0$ in Eq. 43, and using the property that a $3nj$ symbol downgrades to a $(3n-1)j$ symbol when one of its entries is zero. In conclusion, expanding the discussion of Eq. 43 in [14], we suggest that the "screen" for the above $9j$ symbols is three-dimensional, and generalization to higher spin networks should be straight forward.

References

1. Bitencourt, A.C., Marzuoli, A., Ragni, M., Anderson, R.W., Aquilanti, V.: Exact and asymptotic computations of elementary spin networks: Classification of the quantum-classical boundaries. In: Lecture Notes in Computer Science. Volume I-7333., Springer (2012) 723–737 See arXiv:1211.4993[math-ph].
2. Aquilanti, V., Haggard, H.M., Hedeman, A., Jeevanjee, N., Littlejohn, R.G., Yu, L.: Semiclassical mechanics of the Wigner 6j-symbol. J. Phys. A **45**(6) (February 2012) 065209
3. Ragni, M., Bitencourt, A.C., Aquilanti, V., Anderson, R.W., Littlejohn, R.G.: Exact computation and asymptotic approximations of 6j symbols: Illustration of their semiclassical limits. Int. J. Quantum Chem. **110**(3) (2010) 731–742
4. Littlejohn, R.G., Mitchell, K.A., Reinsch, M., Aquilanti, V., Cavalli, S.: Internal spaces, kinematic rotations, and body frames for four-atom systems. Phys. Rev. A **58** (Nov 1998) 3718–3738
5. Aquilanti, V., Bitencourt, A.C.P., da S Ferreira, C., Marzuoli, A., Ragni, M.: Quantum and semiclassical spin networks: from atomic and molecular physics to quantum computing and gravity. Phys. Scripta **78**(5) (2008) 058103
6. Aquilanti, V., Bitencourt, A., da S. Ferreira, C., Marzuoli, A., Ragni, M.: Combinatorics of angular momentum recoupling theory: spin networks, their asymptotics and applications. Theor. Chem. Acc. **123** (2009) 237–247

7. Aquilanti, V., Capecchi, G.: Harmonic analysis and discrete polynomials. from semiclassical angular momentum theory to the hyperquantization algorithm. Theor. Chem. Accounts (104) (2000) 183–188

8. Aquilanti, V., Marinelli, D., Marzuoli, A.: Hamiltonian dynamics of a quantum of space: hidden symmetries and spectrum of the volume operator, and discrete orthogonal polynomials. arXiv:1301.1949v2 [math-ph], J. Phys. A: Math. Theor. **46** (2013) 175303

9. Ragni, M., Littlejohn, R.G., Bitencourt, A.C.P., Aquilanti, V., Anderson, R.W.: The screen representation of spin networks. images of $6j$ symbols and semiclassical features. Lecture Notes in Computer Science **this volume** (2013)

10. Varshalovich, D., Moskalev, A., Khersonskii, V.: Quantum Theory of Angular Momentum. World Scientific, Singapore (1988)

11. Freidel, L., Louapre, D.: Asymptotics of 6j and 10j symbols. Classical and Quantum Gravity **20** (2003) 1267–1294

12. Aquilanti, V., Haggard, H.M., Hedeman, A., Jeevangee, N., Littlejohn, R., Yu, L.: Semiclassical mechanics of the Wigner $6j$-symbol. arXiv:1009.2811v2 [math-ph], J. Phys. A **45**(065209) (2012)

13. Anderson, R.W., Aquilanti, V.: The discrete representation correspondence between quantum and classical spatial distributions of angular momentum vectors. J. Chem. Phys. **124** (2006) 214104 (9 pages)

14. Anderson, R.W., Aquilanti, V., Marzuoli, A.: 3nj morphogenesis and semiclassical disentangling. J. Phys. Chem. A **113** (2009) 15106 – 15117

15. Anderson, R., Aquilanti, V., da S. Ferreira, C.: Exact computation and large angular momentum asymptotics of $3nj$ symbols: semiclassical disentangling of spin-networks. J. Chem. Phys. **129**(161101 (5 pages)) (2008)

16. Neville, D.: A technique for solving recurrence relations approximately and its application to the $3-j$ and $6-j$ symbols. J. Math. Phys. **12** (1971) 2438

17. Schulten, K., Gordon, R.: Semiclassical approximations to 3j- and 6j-coefficients for quantum-mechanical coupling of angular momenta. J. Math. Phys. **16** (1975) 1971–1988

18. Braun, P.A.: Discrete semiclassical methods in the theory of Rydberg atoms in external fields. Rev. Mod. Phys. **65** (January 1993) 115–161

19. Braun, P.: WKB method for three-term recursion relations and quasienergies of an anharmonic oscillator. Sov. Phys. Theor. Math. Phys. **16** (1978) 1070–1081

20. Ponzano, G., Regge, T.: Semiclassical limit of Racah coefficients. Spectroscopic and Group Theoretical Methods in Physics (1968) F. Bloch et al (Eds.), North–Holland, Amsterdam, pp. 1-58.